Impact of metal ns^2 lone pair on luminescence quantum efficiency in low-dimensional halide perovskites

Hongliang Shi,[1] Dan Han,[2,3,4] Shiyou Chen,[2] and Mao-Hua Du[4,*]

[1]*Key Laboratory of Micro-Nano Measurement-Manipulation and Physics (Ministry of Education), Department of Physics, Beihang University, Beijing 100191, China*

[2]*Key Laboratory of Polar Materials and Devices (Ministry of Education), East China Normal University, Shanghai 200241, China*

[3]*Department of Physics, East China Normal University, Shanghai 200241, China*

[4]*Materials Science and Technology Division, Oak Ridge National Laboratory, Oak Ridge, Tennessee 37831, USA*

(Received 13 December 2018; published 12 March 2019)

Based on first-principles calculations, we show that chemically active metal ns^2 lone pairs play an important role in exciton relaxation and dissociation in low-dimensional halide perovskites. We studied excited-state properties of several recently discovered luminescent all-inorganic and hybrid organic-inorganic zero-dimensional (0D) Sn and Pb halides. The results show that, despite the similarity in ground-state electronic structure between Sn and Pb halide perovskites, the chemically more active Sn^{2+} lone pair leads to stronger excited-state structural distortion and larger Stokes shift in Sn halides. The enhanced Stokes shift hinders excitation energy transport, which reduces energy loss to defects and increases the photoluminescence quantum efficiency. The presence of the ns^2 metal cations in the 0D halide perovskites also promotes the exciton dissociation into electron and hole polarons especially in all-inorganic compounds, in which the coupling between metal-halide clusters is significant.

DOI: 10.1103/PhysRevMaterials.3.034604

I. INTRODUCTION

Pb^{2+} and Sn^{2+} based three-dimensional (3D) halide perovskites exhibit excellent carrier transport properties [1–4]. $CH_3NH_3PbI_3$ and related materials have been extensively studied as solar absorber materials [5–9]. The efficient carrier transport in these materials and more generally in ns^2-cation-based halides has been attributed partly to the presence of the ns^2 lone pair, which leads to dispersive valence and conduction bands and a large static dielectric constant [10–14]. The large dielectric constant provides strong screening of charged defects and impurities, leading to shallow defect and impurity levels that do not affect carrier transport significantly [15–18]. In this paper, we show that the chemically active ns^2 lone pair in metal cations also plays an important role in luminescence efficiency in low-dimensional halide perovskites.

Low-dimensional hybrid and all-inorganic halide perovskites have recently attracted intense interest for their rich luminescent properties and potential applications as phosphors and scintillators [19–21]. High photoluminescence quantum efficiency (PLQE) has been reported in many 0D hybrid organic-inorganic halide perovskites [22–24], owing to the radiative recombination of strongly self-trapped excitons (STEs). For example, $(C_4N_2H_{14}Br)_4SnBr_6$ exhibits near-unity PLQE [22]. In these 0D hybrid materials, the anionic metal halide octahedra, which are luminescent centers, are separated from each other by large organic cations. As a result, the STE is not only localized but also immobile, suppressing the exciton migration and the energy loss to defects [25]. Compared to hybrid metal halides, the all-inorganic counterparts could be structurally more stable and, thus, more resilient against defect formation under excitation, which is important to the photostability of phosphors and, especially, scintillators under ionizing radiation. Luminescent properties of all-inorganic 0D halide perovskites have been extensively studied with mixed results. The 0D lead bromide Cs_4PbBr_6 has been studied by many groups for its highly efficient green emission, whose origin, nevertheless, is still under debate [25–29]. The UV emission by STEs in Cs_4PbBr_6 is, however, weak; suffering from strong thermal quenching at $T > 100$ K [30]. At room temperature (RT), the STE emission in Cs_4PbBr_6 is completely quenched. The quenching of the photoluminescence (PL) in Cs_4PbBr_6 was attributed to the exciton migration and the subsequent nonradiative recombination at defects, which are abundant in solution-grown halides [25]. On the other hand, related 0D Eu halide perovskites Cs_4EuX_6 ($X = Br, I$) were shown to be excellent γ-ray scintillators with high light yields at RT [31]. In particular, Cs_4EuBr_6 has the highest light yield under γ-ray excitation among self-activated scintillators. This should be due to the strong exciton localization at Eu^{2+} ions. More recently, Benin *et al.* studied luminescent properties in Cs_4SnX_6 ($X = Br, I$) [32], which are isostructural to Cs_4PbBr_6. Although there is also thermal quenching in Cs_4SnBr_6, it is still highly emissive at RT with PLQE of 15 $\pm$ 5%. Increasing the iodine concentration in $Cs_4Sn(Br_{1-x}I_x)_6$ leads to the quenching of the PL at $x = 0.5$. Cs_4SnI_6 is not emissive at RT. As can be seen, the luminescence efficiency in these 0D halide perovskites varies strongly with the chemical composition (especially with the type of the metal ion). Understanding the material chemistry that underpins the different optical properties in 0D metal halides will enable the

*Corresponding author: mhdu@ornl.gov

development of more effective property tuning and optimization methods and the design of highly efficient luminescent materials.

In this paper, we performed density functional theory (DFT) calculations with hybrid functionals to study electronic structure as well as exciton and polaron properties in Sn and Pb-based 0D halide perovskites, i.e., Cs_4SnX_6 ($X = Br, I$), Cs_4PbBr_6, and R_4SnBr_6 ($R = C_4N_2H_{14}Br$) . We show that the different PL efficiencies and the different thermal quenching behaviors between 0D Sn and Pb halides lie in the different lone-pair reactivities between Sn^{2+} and Pb^{2+}. In comparison to Cs_4PbBr_6, the more chemically active Sn^{2+} in Cs_4SnBr_6 leads to stronger local structural distortion at the excited state. This gives rise to a larger Stokes shift in Cs_4SnBr_6, which in turn limits the exciton migration and energy loss to defects. We further show that the dissociation of excitons into electron and hole polarons in Cs_4SnX_6 ($X = Br, I$), Cs_4PbBr_6, and R_4SnBr_6 is energetically possible at RT, which is also related to the lone-pair chemistry of Sn^{2+} and Pb^{2+} .

II. COMPUTATIONAL METHODS

All calculations were based on DFT implemented in the VASP code (version 5.3.5) [33]. The interaction between ions and electrons was described by the projector augmented wave method [34]. Electronic band structures, density of states (DOS), excitons, and polarons were studied by using the hybrid PBE0 functional [35]. Spin-orbit coupling (SOC) was included in the calculations on Cs_4PbBr_6 because it was shown previously that the SOC has a strong effect on the Pb-6p-derived conduction band [36]. More computational details are available in the Supplemental Material [37].

Following the Franck-Condon principle, the exciton excitation and emission energies were obtained by calculating the total energy differences between the excited and the ground states using PBE0-optimized ground-state and excited-state structures, respectively. For Sn compounds, a spin-singlet exciton was considered when calculating the excitation energy because this is a spin-allowed transition, while a spin-triplet exciton was considered for calculating the emission energy because the spin-triplet exciton is more stable than the spin-singlet one. The slow PL decay on the order of microsecond observed for Cs_4SnBr_6 and $(C_4N_2H_{14}Br)_4SnBr_6$ [22,32] is consistent with the spin-forbidden transition for the radiative recombination of the spin-triplet exciton. For Cs_4PbBr_6, there is strong mixing between the spin-singlet and -triplet states of the exciton due to the strong SOC effect on Pb; thus, the SOC was included in the exciton calculations. The exciton binding energy (relative to a free electron and free hole) was calculated by $\Delta E_b = E(\mathrm{GS}) + E_g - E(\mathrm{exciton})$, where E(GS) and E(exciton) are the total energies of the ground state and the exciton, respectively, and E_g is the band gap.

The total energy of an exciton was calculated by fixing the occupation numbers of the electron and hole-occupied eigenlevels [Δ self-consistent field (ΔSCF) method [38–40]]. The ΔSCF method can be easily used here because the electron and hole are both localized on a single inorganic cluster and each occupies one single eigenlevel deep inside the band gap [25]. Such localized electron and hole levels are found for both spin-singlet and -triplet excitons with or without structural distortion in all four compounds studied in this paper. The ΔSCF method combined with the hybrid PBE0 functional has shown accurate results in exciton excitation and emission energies in low-dimensional halide perovskites [21,23,25,41,42].

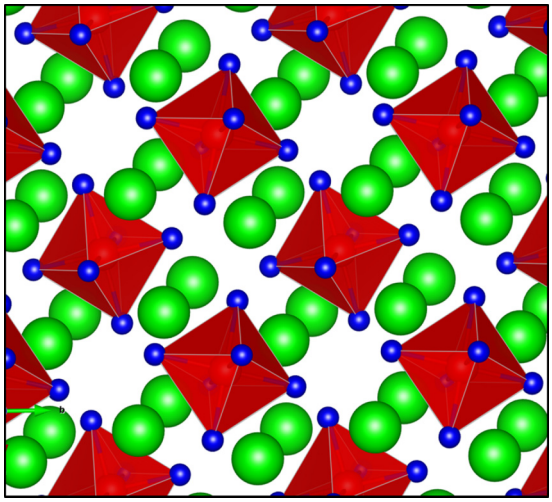

FIG. 1. Crystal structure of Cs_4SnBr_6, Cs_4SnI_6, and Cs_4PbBr_6, which have the same space group R-3C (#167). The green and blue balls represent Cs and Br ions, respectively. The red balls at the center of each octahedron represent Sn or Pb.

III. RESULTS AND DISCUSSION

A. Electronic structure

We first compare the electronic band structures of Cs_4SnBr_6, Cs_4SnI_6, and Cs_4PbBr_6, which share the same crystal structure as shown in Fig. 1. The Sn compounds have somewhat more dispersive conduction and valence bands than the Pb compound as can be seen in Fig. 2. More dispersive bands usually lead to less localized and more mobile excitons and lower PL efficiencies. However, this is not the case here as the exciton emission in Cs_4SnBr_6 is more efficient than that in Cs_4PbBr_6, which is to be explained below.

The Pb-6p-derived conduction band of Cs_4PbBr_6 is split off from other higher-energy Pb-6p bands by the SOC. The conduction band of Cs_4PbBr_6 obtained without the SOC resembles that of Cs_4SnBr_6. The ns^2 lone pair (Sn-5s or Pb-6s) levels are below the valence band and hybridize with the halogen p levels in the valence band. The bonding orbitals between the ns^2 lone pair and halogen-p orbitals form a narrow band below the valence band [located near -6.5 eV (Cs_4SnBr_6), -6.55 eV (Cs_4SnI_6), and -7.3 eV (Cs_4PbBr_6) (Figure S1)] [37]. The valence band of these compounds has three components. Taking Cs_4SnBr_6 as an example, the band near -3 eV is made up of bonding orbitals between Sn-5p and Br-4p as shown in Fig. 2(b); the top valence band near 0 eV is made up of antibonding orbitals between Sn-5s and Br-4p; the band between the above two is a mixing of Br-4p orbitals that are not hybridized with Sn orbitals and is, therefore, termed the nonbonding Br-4p band. (Note that the orbital makeup of electronic bands can be seen in the projected DOS in

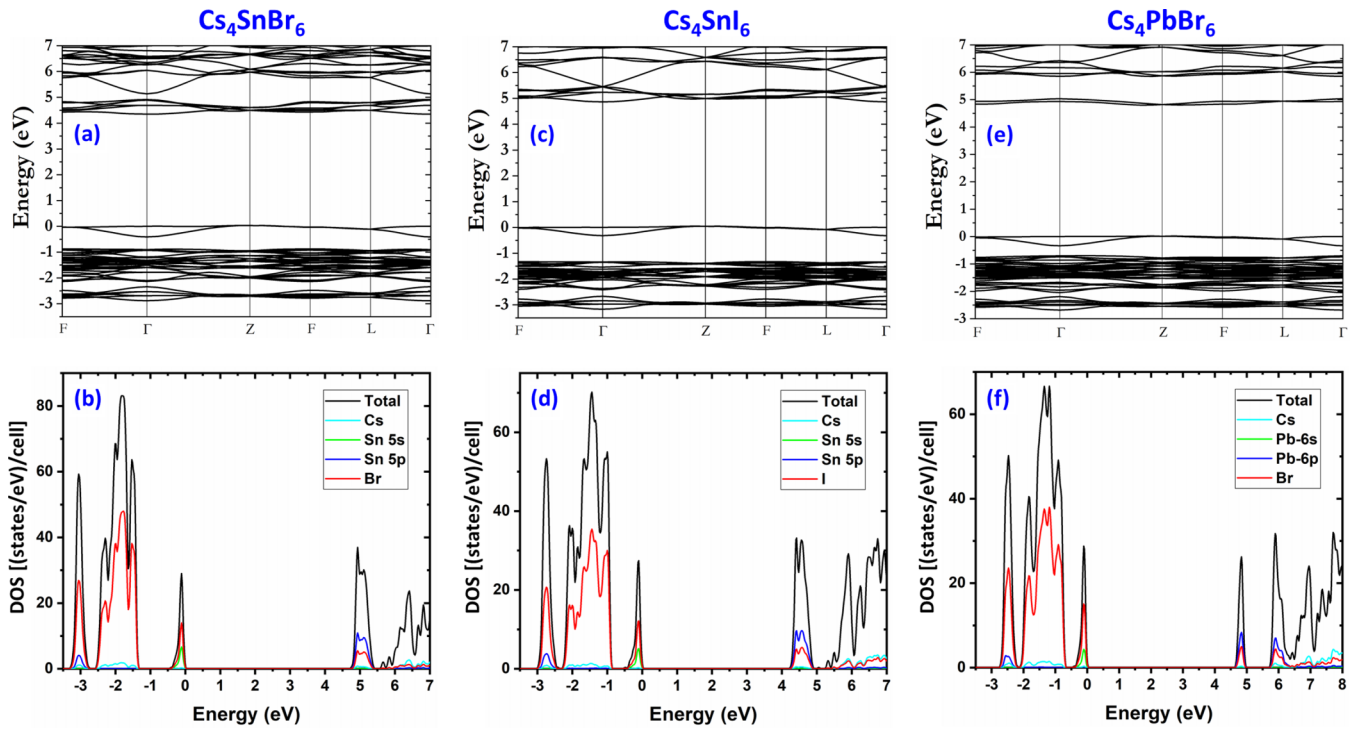

FIG. 2. Electronic band structures and DOS of (a), (b) Cs_4SnBr_6, (c), (d) Cs_4SnI_6, and (e), (f) Cs_4PbBr_6 obtained by PBE0 calculations. The SOC is included only for (e), (f) Cs_4PbBr_6. The DOS is projected to each atomic species. The DOS with a wider energy scale showing the band derived primarily from the ns^2 lone pairs (Sn-5*s* or Pb-6*s*) is shown in Fig. S1 [37].

Fig. 2.) The energy splitting between the top valence band and the nonbonding halogen- *p* band indicates the hybridization strength between the metal ns^2 lone pair and the halogen *p* orbitals. This splitting is largest in Cs_4SnBr_6 (1.01 eV) followed by Cs_4SnI_6 (0.46 eV) and Cs_4PbBr_6 (0.36 eV) as shown in Fig. 2. Therefore, the hybridization between the metal ns^2 lone pair and the halogen *p* orbital is strongest in Cs_4SnBr_6, followed by Cs_4SnI_6 and Cs_4PbBr_6. This can be understood by the following. Br-4*p* orbitals have stronger hybridization with the Sn-5*s* lone pair in Cs_4SnBr_6 than the I-5*p* orbitals in Cs_4SnI_6 because Br-4*p* levels are lower and closer in energy to the Sn-5*s* level than I-5*p* levels. The Pb-6*s*-Br-4*p* hybridization in Cs_4PbBr_6 is relatively weak because the Pb-6*s* level is lower in energy than the Sn-5*s* level [43] and is more inert (so-called "inert pair effect") [44,45]. The inert pair effect of Pb 6*s* arises from the relativistic contraction of *s* orbitals, which is significant in heavy elements, such as Pb. [44,45] Such orbital contraction is evidenced by the relatively low Pb-6*s* level and short Pb-Br bond length. The Pb-6*s*-derived band in Cs_4PbBr_6 is about 7.3 eV below the valence band maximum (VBM), while the Sn-5*s*-derived band in Cs_4SnBr_6 is about 6.5 eV below the VBM (see Figure S1 [37]). The calculated Pb-Br bond length (3.04 Å) in Cs_4PbBr_6 is very close to the calculated Sn-Br bond length (3.00 Å) in Cs_4SnBr_6 despite that Pb^{2+} is a 6*s* ion, while Sn^{2+} is a 5*s* ion. Comparing Sn^{2+} and Pb^{2+} based halides, it is well known that Sn^{2+} is prone to oxidation while Pb^{2+} is much more stable [46]; this is the reason for the significantly lower efficiency of $CH_3NH_3SnI_3$ solar cells [47,48] than that of $CH_3NH_3SnPbI_3$ solar cells [5]. The strong antibonding character of the top valance band in Cs_4SnBr_6 has important consequences in the excited-state structural relaxation and optical properties as discussed below.

The calculated valence band width (0.37 eV) in Cs_4SnBr_6 is slightly larger than that in Cs_4PbBr_6 (0.35 eV). This small difference is consistent with the small difference in the shortest intercluster Br-Br distance (4.09 vs 4.07 Å) in Cs_4SnBr_6 and Cs_4PbBr_6. Thus, the intercluster coupling strength at the ground state cannot explain the bright luminescent Cs_4SnBr_6 and the nonemissive Cs_4PbBr_6 at RT. The valence band width of Cs_4SnI_6 is larger at 0.44 eV; this is likely due to the closer contact between larger-sized I ions.

B. Exciton properties and enhanced PLQE by large Stokes shift

Figure 3 shows the calculated binding energies of unrelaxed and relaxed excitons (relative to free carriers) in Cs_4SnX_6 (X = Br, I), Cs_4PbBr_6, and R_4SnBr_6. The binding of the unrelaxed exciton in Cs_4PbBr_6 (−1.17 eV) and R_4SnBr_6 (−1.25 eV) is stronger than that in Cs_4SnX_6 (X = Br, I) (−0.92 and −0.82 eV); the stronger binding of unrelaxed excitons in the former two compounds is largely the result of narrower conduction and valence bands (see band structures in Fig. 2 and Ref. [25]). However, after exciton relaxation, the exciton binding energy of Cs_4PbBr_6 (−1.25 eV) becomes significantly weaker than that in Cs_4SnX_6 (X = Br, I) and R_4SnBr_6 (−1.86, −1.62, and −2.23 eV, respectively), indicating much stronger excited-state structural relaxation in the three Sn halides (Fig. 3). (The relaxed structures of excitons in all four compounds can be found in the Supplemental Material [37].) The binding of the unrelaxed and relaxed excitons in R_4SnBr_6 are both strong, reflecting the fact of

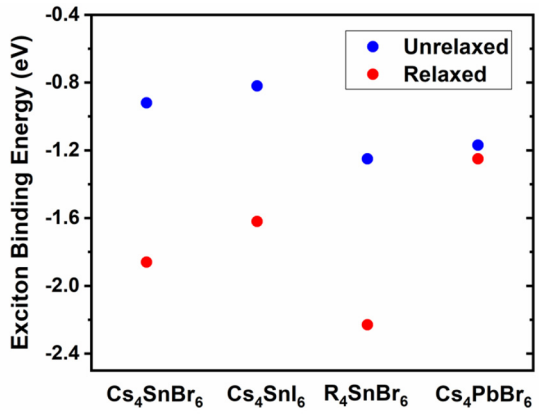

	Cs_4SnBr_6	Cs_4SnI_6	R_4SnBr_6	Cs_4PbBr_6
ΔE_{Relax} (eV)	0.94	0.80	0.98	0.08

FIG. 3. Binding energies of unrelaxed and relaxed excitons relative to free electron and hole, as well as the exciton relaxation energy (ΔE_{Relax}), which is the difference between the former two binding energies, in Cs_4SnBr_6, Cs_4SnI_6, R_4SnBr_6, and Cs_4PbBr_6. A negative binding energy indicates stable binding.

both narrow bands and strong exciton relaxation. In these 0D compounds, the exciton localization is strongly favored even in unrelaxed excitons; the key to the understanding of the different exciton emission efficiencies is the mobility (rather than the localization) of the excitons as discussed below.

The calculated exciton excitation/emission energies and Stokes shifts in 0D Sn and Pb halide perovskites are in good agreement with the available experimental values as shown in Fig. 4. As a result of the weak exciton relaxation in Cs_4PbBr_6, the calculated Stokes shift in Cs_4PbBr_6 (0.58 eV) is much smaller than those in the three Sn compounds (1.45–1.76 eV). A large Stokes shift can reduce the spectral overlap between the excitation and emission; thus, limiting the resonant transfer of excitation energy [25,49,50].

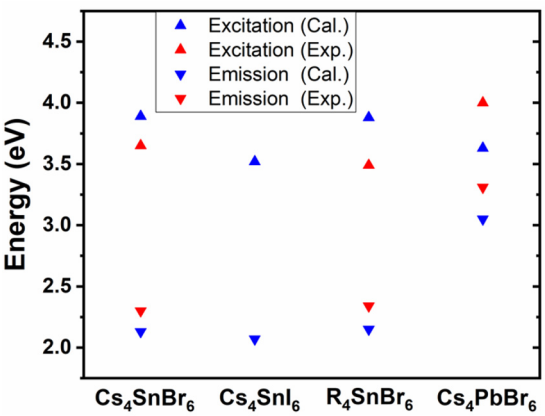

Stokes Shift (eV)	Cs_4SnBr_6	Cs_4SnI_6	R_4SnBr_6	Cs_4PbBr_6
Calculation	1.76	1.45	1.73	0.58
Experiment	1.35	N/A	1.15	0.69

FIG. 4. Calculated and experimentally measured exciton excitation and emission energies and the Stokes shifts in Cs_4SnBr_6, Cs_4SnI_6, R_4SnBr_6, and Cs_4PbBr_6.

If the resonant condition is not satisfied, the exciton transfer would require phonon assistance, which significantly reduces the energy transport efficiency. The suppression of exciton migration reduces the probability for an exciton to encounter defects, thereby, reducing the nonradiative recombination rate. Increasing temperature broadens the excitation and emission bands. For Cs_4SnBr_6 at RT, the tails of the two bands touch each other despite a large measured Stokes shift of 1.35 eV [32]. The measured Stokes shift in Cs_4PbBr_6 is only 0.69 eV [30], which is too small to prevent the spectral overlap as the temperature rises. This explains the highly emissive STE in Cs_4SnBr_6 [32] as opposed to the absence of STE emission in Cs_4PbBr_6 at RT [30].

The calculated Stokes shift in Cs_4SnI_6 (1.45 eV) is smaller than that in Cs_4SnBr_6 (1.76 eV). The excitation and emission bands of Cs_4SnI_6 are also expected to be broader than those in Cs_4SnBr_6 due to the generally softer phonons in iodides than in bromides. Thus, Cs_4SnI_6 should suffer from stronger thermal quenching of PL than Cs_4SnBr_6, as a result of spectral overlap and resonant excitonic energy transfer. This is consistent with the experimental observation that increasing the iodine concentration in $Cs_4Sn(Br_{1-x}I_x)_6$ leads to the quenching of the RT PL at $x = 0.5$.

C. Effects of ns^2 lone pair reactivity on exciton relaxation and Stokes shift

As discussed above in Sec. III B, a large Stokes shift enhances exciton emission efficiency. Below we show that the reactivity of the ns^2 lone pair has a strong impact on the excited-state structural relaxation and the Stokes shift. To demonstrate this point, we compare the structures of the STEs in Cs_4SnBr_6 and Cs_4PbBr_6, which differ only by the type of the ns^2 cation. In Cs_4SnBr_6, the exciton localization at a $(SnBr_6)^{2-}$ octahedron causes the contraction of the four Sn-Br bonds in the $SnBr_4$ plane (due to the hole localization centered at Sn) and the elongation of the two Sn-Br bonds perpendicular to the plane (due to the electron localization on a Sn-5p orbital) [25]. The patterns of the bond length changes in excited states of all four compounds are similar as illustrated in Fig. 5; however, the extents of relaxation are different. The top valence band of Cs_4SnBr_6 has a stronger antibonding character (between the Sn-5s lone pair and Br-4p) than that of Cs_4PbBr_6 (between the Pb-6s lone pair and Br-4p) as a result of the chemically more active Sn-5s lone pair than the Pb-6s lone pair (a relativistic effect described above in Sec. III A). Consequently, creating a hole at the top of the valence band leads to stronger bond contraction in Cs_4SnBr_6 than in Cs_4PbBr_6 as shown in Fig. 5. The four in-plane metal-Br bonds contract significantly from 3.00 to 2.78 Å (7.3%) in Cs_4SnBr_6 and, to a much lesser extent, from 3.04 to 2.93 Å (3.6%) in Cs_4PbBr_6. The stronger inward contraction of the four in-plane Br anions in Cs_4SnBr_6 should further promote a stronger outward relaxation of the two Br ions on the two vertical bonds due to the Br-Br repulsion. Indeed, the increase of the two vertical Sn-Br bond lengths in Cs_4SnBr_6 [from 3.00 to 3.57 Å (19.0%)] is larger than that of the Pb-Br bonds in Cs_4PbBr_6 [from 3.04 to 3.52 Å (15.8%)]. Due to the stronger excited-state structural relaxation in Cs_4SnBr_6, the calculated exciton relaxation energy in Cs_4SnBr_6 (0.94 eV) is much

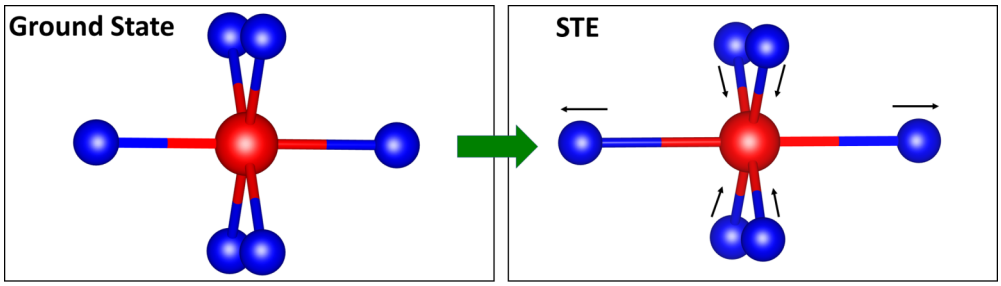

STE Structure	Cs_4SnBr_6	Cs_4SnI_6	R_4SnBr_6	Cs_4PbBr_6
Four Short Bonds	-7.3%	-6.0%	-9.9%	-3.6%
Two Long Bonds	+19.0%	+16.0%	+19.8%	+15.8%

FIG. 5. Structure distortion (indicated by black arrows) caused by the STE formation in Cs_4SnBr_6, Cs_4SnI_6, R_4SnBr_6, and Cs_4PbBr_6.

larger than that in Cs_4PbBr_6 (0.08 eV) (Fig. 3), which leads to the larger calculated Stokes shift in Cs_4SnBr_6 (1.76 eV) than in Cs_4PbBr_6 (0.58 eV) (Fig. 4).

D. Stability of excitons relative to polarons

It is shown above that the calculated exciton binding energies relative to free carriers are large for all four 0D metal halides studied here. However, the calculated exciton binding relative to two isolated electron and hole polarons is weak; the binding energies for Cs_4SnBr_6, Cs_4SnI_6, R_4SnBr_6, and Cs_4PbBr_6 are 0, −0.19, −0.09, −0.04 eV, respectively (see Fig. 6). Moreover, a polaron pair (an electron and a hole polaron localized on two adjacent metal-halogen octahedra) is more stable than a STE by 0.21 eV (Cs_4PbBr_6), 0.17 eV (Cs_4SnBr_6), 0.04 eV (Cs_4SnI_6), and 0.08 eV (R_4SnBr_6). The unusual stability of polarons relative to a STE is also related to the ns^2 metal cation. An electron in a STE or in an electron polaron is always localized on a metal-*p* orbital, causing the elongation of two metal-halogen bonds (as illustrated in Fig. 5). However, the hole localization in a STE and in a hole polaron causes different types of structural distortion. In a STE, the hole distributed at the metal-*s* orbital (which leads to a more positively charged metal cation) reduces the lengths of four metal-halogen bonds (Fig. 5). On the other hand, when the electron and hole in a STE are separated to two polarons on two metal-halide octahedra, the hole centered at a ns^2 cation attract all six halogen anions in the octahedron, leading to six shortened metal-halogen bonds in the hole polaron (rather than four shortened bonds in the case of a STE). This additional Coulomb energy gain compensates for the energy loss due to the separation of the electron and the hole. Using Cs_4SnBr_6 as an example, the Sn-Br bond length at the ground state is 3.00 Å. In a STE localized at a $SnBr_6$ octahedron, the Sn-Br bond lengths of the two long bonds and the four short bonds are 3.57 and 2.78 Å, respectively. In comparison, in an isolated hole polaron, all six Sn-Br bonds are short bonds with an average length of 2.79 Å; in an isolated electron polaron, the two long Sn-Br bonds have an average bond length of 3.67 Å and the other four bonds have an average length of 3.06 Å.

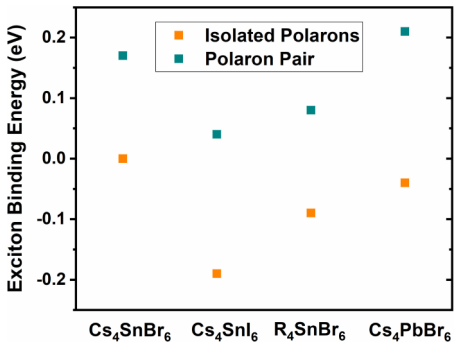

FIG. 6. Exciton binding energies relative to isolated electron and hole polarons as well as to electron-hole polaron pairs in Cs_4SnBr_6, Cs_4SnI_6, R_4SnBr_6, and Cs_4PbBr_6. A negative binding energy indicates stable binding.

This above analysis reveals that the stability of polarons relative to a STE in 0D halide perovskites containing ns^2 cations is related to the fact that the localized electron and hole are both centered at the ns^2 cation. If the metal ion in the center of the octahedron is not a ns^2 ion such that the hole localization is not centered at the metal cation but rather causes the formation of a halogen-halogen bond (a V_k center) [51], the hole would be localized on the halogen-halogen bond, while the electron is localized on at the adjacent metal cation that binds the hole. In this case, there is no energy incentive to separate the electron from the hole.

In the above 0D halide perovskites, without structural distortion, an exciton can be localized at one cluster by strong Coulomb binding, while the formation of an electron-hole polaron pair is energetically unfavorable. The polaron stabilization must involve strong structural distortion. Thus, optical excitation of an electron-hole pair should lead to an exciton localized on one metal halide cluster rather than a polaron pair on two adjacent clusters. The subsequent excited-state relaxation could lead to a polaron pair if the electron can tunnel to the adjacent cluster, which is subject to a kinetic barrier. The tunneling of an electron polaron from one cluster to another to separate from the hole is more difficult than the exciton tunneling due to the Coulomb binding between the electron and the hole. Even without the Coulomb binding, the diffusion of a charged polaron is in general more difficult and subject to a higher kinetic barrier than the diffusion of a neutral exciton [52]. The polaron tunneling between two adjacent clusters should also require more phonon assistance than the exciton tunneling because, without structure distortion, an electron

would prefer delocalization, whereas an exciton still prefers localization due to Coulomb binding. Therefore, increasing temperature is expected to first enable exciton diffusion before the exciton dissociation into polaron pairs becomes possible. We have also calculated the emission energy of a polaron pair in Cs_4PbBr_6, which yields 1.79 eV, much lower than the STE emission energy >3 eV (Fig. 4). This shows that the experimentally observed emission is due to the STE localized at one metal-halide cluster rather than the polaron pairs distributed at two adjacent clusters. In all-inorganic Cs_4PbBr_6, Cs_4SnBr_6, and Cs_4SnI_6, there is relatively strong electronic and vibrational intercluster coupling, which may enable the STE dissociation, providing another channel for PL thermal quenching (in addition to the STE diffusion and trapping at defects). In hybrid R_4SnBr_6, where the $SnBr_6$ clusters are decoupled by large-sized organic molecules, the STE diffusion and separation are both suppressed; thus, giving rise to a near-unity PLQE [22,25].

IV. SUMMARY

This work provides an important understanding of the effect of the metal ns^2 lone pair on exciton relaxation and dissociation, which determine the luminescence efficiency, in 0D halide perovskites. We performed hybrid DFT calculations to study exciton emission in 0D Sn and Pb halide perovskites, Cs_4SnX_6 (X = Br, I), Cs_4PbBr_6, and R_4SnBr_6, which contain ns^2 metal cations (Sn^{2+} and Pb^{2+}). By comparing the Sn^{2+} and Pb^{2+} based compounds, we show that the chemically more active Sn-5s lone pair gives rise to stronger hole-induced excited-state structural distortion and larger Stokes shift. The large Stokes shift in 0D Sn halides hinders the resonant transport of excitation energy; thus, reducing energy loss to defects, which are usually abundant in these solution-grown halides. This explains the generally higher PLQE in 0D Sn halide perovskites than in Pb halides and their thermal quenching behaviors. Our calculations also show that the presence of ns^2 metal cations promotes the exciton dissociation into electron and hole polarons in 0D Sn and Pb halide perovskites especially in all-inorganic compounds, in which the coupling between the metal-halide clusters is significant. The separation of the electron and the hole should reduce the efficiency of exciton radiative recombination, providing another mechanism for PL quenching. Our results suggest that the key factor to a high PLQE in 0D halide perovskites is the suppression of exciton and polaron tunneling between inorganic clusters, which are luminescent centers, by a weak intercluster coupling and/or a large Stoke shift.

ACKNOWLEDGMENTS

The work at ORNL were supported by the U.S. Department of Energy, Office of Science, Basic Energy Sciences, Materials Sciences and Engineering Division. H.S. was supported by the National Natural Science Foundation of China (NSFC) under Grants No.11604007 and the start-up funding at Beihang University. D.H. and S.C. were supported by the State Scholarship Fund in China and CC of ECNU.

[1] Q. Dong, Y. Fang, Y. Shao, P. Mulligan, J. Qiu, L. Cao, and J. Huang, Science **347**, 967 (2015).
[2] S. D. Stranks, G. E. Eperon, G. Grancini, C. Menelaou, M. J. P. Alcocer, T. Leijtens, L. M. Herz, A. Petrozza, and H. J. Snaith, Science **342**, 341 (2013).
[3] G. Xing, N. Mathews, S. Sun, S. S. Lim, Y. M. Lam, M. Grätzel, S. Mhaisalkar, and T. C. Sum, Science **342**, 344 (2013).
[4] D. Shi, V. Adinolfi, R. Comin, M. Yuan, E. Alarousu, A. Buin, Y. Chen, S. Hoogland, A. Rothenberger, K. Katsiev, Y. Losovyj, X. Zhang, P. A. Dowben, O. F. Mohammed, E. H. Sargent, and O. M. Bakr, Science **347**, 519 (2015).
[5] M. A. Green, A. Ho-Baillie, and H. J. Snaith, Nat. Photonics **8**, 506 (2014).
[6] J. Berry, T. Buonassisi, D. A. Egger, G. Hodes, L. Kronik, Y.-L. Loo, I. Lubomirsky, S. R. Marder, Y. Mastai, and J. S. Miller, D. B. Mitzi, Y. Paz, A. M. Rappe, I. Riess, B. Rybtchinski, O. Stafsudd, V. Stevanovic, M. F. Toney, D. Zitoun, A. Kahn, D. Ginley and D. Cahen, Adv. Mater. **27**, 5102 (2015).
[7] C. Zuo, H. J. Bolink, H. Han, J. Huang, D. Cahen, and L. Ding, Adv. Sci. **3**, 1500324 (2016).
[8] https://www.nrel.gov/ncpv/images/efficiency_chart.jpg.
[9] N.-G. Park, MRS Bull. **43**, 527 (2018).
[10] M.-H. Du and D. J. Singh, Phys. Rev. B **81**, 144114 (2010).
[11] M.-H. Du and D. J. Singh, Phys. Rev. B **82**, 045203 (2010).
[12] M. H. Du, J. Mater. Chem. A **2**, 9091 (2014).
[13] R. E. Brandt, V. Stevanović, D. S. Ginley, and T. Buonassisi, MRS Commun. **5**, 265 (2015).
[14] L.-y. Huang and W. R. L. Lambrecht, Phys. Rev. B **88**, 165203 (2013).
[15] M. H. Du, J. Phys. Chem. Lett. **6**, 1461 (2015).
[16] H. Shi and M.-H. Du, Phys. Rev. B **90**, 174103 (2014).
[17] W.-J. Yin, T. Shi, and Y. Yan, Appl. Phys. Lett. **104**, 063903 (2014).
[18] A. Buin, P. Pietsch, J. Xu, O. Voznyy, A. H. Ip, R. Comin, and E. H. Sargent, Nano Lett. **14**, 6281 (2014).
[19] H. Lin, C. Zhou, Y. Tian, T. Siegrist, and B. Ma, ACS Energy Lett. **3**, 54 (2018).
[20] M. D. Smith and H. I. Karunadasa, Accounts Chem. Res. **51**, 619 (2018).
[21] C. Zhou, H. Lin, Q. He, L. Xu, M. Worku, M. Chaaban, S. Lee, X. Shi, M.-H. Du, and B. Ma, Mater. Sci. Eng. Rep. **137**, 38 (2019).
[22] C. Zhou, H. Lin, Y. Tian, Z. Yuan, R. J. Clark, B. Chen, L. J. van de Burgt, J. C. Wang, Y. Zhou, K. Hanson, Q. Meisner, J. Neu, T. Besara, T. Siegrist, E. Lambers, P. I. Djurovich, and B. Ma, Chem. Sci. **9**, 586 (2018).
[23] C. Zhou, M. Worku, J. Neu, H. Lin, Y. Tian, S. Lee, Y. Zhou, D. Han, S. Chen, A. Hao, P. I. Djurovich, T. Siegrist, M.-H. Du, and B. Ma, Chem. Mat. **30**, 2374 (2018).
[24] C. Zhou, H. Lin, M. Worku, J. Neu, Y. Zhou, Y. Tian, S. Lee, P. Djurovich, T. Siegrist, and B. Ma, J. Am. Chem. Soc. **140**, 13181 (2018).
[25] D. Han, H. Shi, W. Ming, C. Zhou, B. Ma, B. Saparov, Y.-Z. Ma, S. Chen, and M.-H. Du, J. Mater. Chem. C **6**, 6398 (2018).

[26] Q. A. Akkerman, A. L. Abdelhady, and L. Manna, J. Phys. Chem. Lett. **9**, 2326 (2018).
[27] X. Chen, F. Zhang, Y. Ge, L. Shi, S. Huang, J. Tang, Z. Lv, L. Zhang, B. Zou, and H. Zhong, Adv. Funct. Mater. **28**, 1706567 (2018).
[28] J. Yin, H. Yang, K. Song, A. M. El-Zohry, Y. Han, O. M. Bakr, J.-L. Brédas, and O. F. Mohammed, J. Phys. Chem. Lett. **9**, 5490 (2018).
[29] M. Hu, C. Ge, J. Yu, and J. Feng, J. Phys. Chem. C **121**, 27053 (2017).
[30] M. Nikl, E. Mihokova, K. Nitsch, F. Somma, C. Giampaolo, G. P. Pazzi, P. Fabeni, and S. Zazubovich, Chem. Phys. Lett. **306**, 280 (1999).
[31] Y. Wu, D. Han, B. C. Chakoumakos, H. Shi, S. Chen, M.-H. Du, I. Greeley, M. Loyd, D. J. Rutstrom, L. Stand, M. Koschan, and C. L. Melcher, J. Mater. Chem. C **6**, 6647 (2018).
[32] B. M. Benin, D. N. Dirin, V. Morad, M. Wörle, S. Yakunin, G. Rainò, O. Nazarenko, M. Fischer, I. Infante, and M. V. Kovalenko, Angew. Chem. Int. Edit. **57**, 11329 (2018).
[33] G. Kresse and J. Furthmüller, Comp. Mater. Sci. **6**, 15 (1996).
[34] G. Kresse and D. Joubert, Phys. Rev. B **59**, 1758 (1999).
[35] J. P. Perdew, M. Emzerhof, and K. Burke, J. Chem. Phys. **105**, 9982 (1996).
[36] J. Even, L. Pedesseau, J.-M. Jancu, and C. Katan, J. Phys. Chem. Lett. **4**, 2999 (2013).
[37] See Supplemental Material at http://link.aps.org/supplemental/10.1103/PhysRevMaterials.3.034604 for computational details, DOS, and STE structures.
[38] R. O. Jones and O. Gunnarsson, Rev. Mod. Phys. **61**, 689 (1989).
[39] A. Görling, Phys. Rev. A **59**, 3359 (1999).
[40] A. Hellman, B. Razaznejad, and B. I. Lundqvist, J. Chem. Phys. **120**, 4593 (2004).
[41] C. Zhou, H. Lin, H. Shi, Y. Tian, C. Pak, M. Shatruk, Y. Zhou, P. Djurovich, M.-H. Du, and B. Ma, Angew. Chem. Int. Edit. **57**, 1021 (2018).
[42] G. Wu, C. Zhou, W. Ming, D. Han, S. Chen, D. Yang, T. Besara, J. Neu, T. Siegrist, M.-H. Du, B. Ma, and A. Dong, ACS Energy Lett. **3**, 1443 (2018).
[43] L.-D. Yuan, H.-X. Deng, S.-S. Li, S.-H. Wei, and J.-W. Luo, Phys. Rev. B **98**, 245203 (2018).
[44] P. Pyykko, Chem. Rev. **88**, 563 (1988).
[45] P. Pyykko and J. P. Desclaux, Acc. Chem. Res. **12**, 276 (1979).
[46] T. Yokoyama, D. H. Cao, C. C. Stoumpos, T.-B. Song, Y. Sato, S. Aramaki, and M. G. Kanatzidis, J. Phys. Chem. Lett. **7**, 776 (2016).
[47] F. Hao, C. C. Stoumpos, D. H. Cao, R. P. H. Chang, and M. G. Kanatzidis, Nat. Photon **8**, 489 (2014).
[48] N. K. Noel, S. D. Stranks, A. Abate, C. Wehrenfennig, S. Guarnera, A.-A. Haghighirad, A. Sadhanala, G. E. Eperon, S. K. Pathak, M. B. Johnston, A. Petrozza, L.M. Herz, and H. J. Snaith, Energy Environ. Sci. **7**, 3061 (2014).
[49] G. Blasse and B. C. Grabmaier, *Luminescent Materials* (Springer-Verlag, Berlin,1994).
[50] D. L. Dexter, J. Chem. Phys. **21**, 836 (1953).
[51] K. Biswas and M. H. Du, Phys. Rev. B **86**, 014102 (2012).
[52] K. S. Song and R. T. Williams, *Self-Trapped Excitons* (Springer-Verlag, Berlin, 1996).